

WEAK-SCALE PHENOMENOLOGY IN MODELS WITH  
GAUGE-MEDIATED SUPERSYMMETRY BREAKINGJONATHAN A. BAGGER,<sup>a</sup>  
KONSTANTIN MATCHEV,<sup>a</sup>  
DAMIEN M. PIERCE<sup>b</sup> and  
RENJIE ZHANG<sup>a</sup><sup>a</sup> *Department of Physics and Astronomy  
Johns Hopkins University  
3400 N. Charles Street  
Baltimore, Maryland 21218*<sup>b</sup> *Stanford Linear Accelerator Center  
Stanford University  
Stanford, California 94309***Abstract**

We study in some detail the spectral phenomenology of models in which supersymmetry is dynamically broken and transmitted to the supersymmetric partners of the quarks, leptons and gauge bosons, and the Higgs bosons themselves, via the usual gauge interactions. We elucidate the parameter space of what we consider to be the minimal model, and explore the regions which give rise to consistent radiative electroweak symmetry breaking. We include the weak-scale threshold corrections, and show how they considerably reduce the scale dependence of the results. We examine the sensitivity of our results to unknown higher-order messenger-sector corrections. We compute the superpartner spectrum across the entire parameter space, and compare it to that of the minimal supergravity-inspired model. We delineate the regions where the lightest neutralino or tau slepton is the next-to-lightest supersymmetric particle, and compute the lifetime and branching ratios of the NLSP. In contrast to the minimal supergravity-inspired model, we find that the lightest neutralino can have a large Higgsino component, of order 50%. Nevertheless, the neutralino branching fraction to the gravitino and the light Higgs boson remains small,  $\lesssim 10^{-4}$ , so the observation of such a decay would point to a non-minimal Higgs sector.

# 1 Introduction

Most studies of supersymmetric phenomenology have focused on models in which supersymmetry is broken in a hidden sector at a scale of order  $M_{\text{SUSY}} \simeq 10^{10}$  GeV. In these models, supersymmetry breaking is communicated to the visible sector by gravitational interactions. Such models give rise to superpartner masses in the 100 – 1000 GeV range, and to a gravitino with approximately the same mass. The couplings of the gravitino to matter are negligible, suppressed by  $(E/M_{\text{SUSY}})^2 \simeq 10^{-16}$ . The now-standard “minimal supergravity” model is of this type, with the familiar unification-scale boundary conditions on  $M_0$ ,  $M_{1/2}$ , and  $A_0$ .

Recently, there has been a resurgence of interest in models where supersymmetry is broken at a scale of order  $M_{\text{SUSY}} \gtrsim 10^5$  GeV [1] – [11]. In these models, supersymmetry breaking is transmitted to the superpartners of the quarks, leptons, and gauge bosons (and to the Higgs bosons themselves) via the usual  $\text{SU}(3) \times \text{SU}(2) \times \text{U}(1)$  gauge interactions. Because gauge interactions are flavor diagonal, these models naturally suppress the flavor-changing neutral currents associated with the soft squark and slepton masses.

Models with gauge-mediated symmetry breaking also have superpartner masses in the 100 – 1000 GeV range. However, because of the low scale of supersymmetry breaking, the gravitino is essentially massless; its couplings to the superpartners are suppressed by  $(E/M_{\text{SUSY}})^2 \lesssim 10^{-6}$ . Typically, superparticles decay by cascading down to the next-to-lightest supersymmetric particle (NLSP), which in turn decays to its partner and the gravitino. Such decays give rise to characteristic experimental signatures, e.g. final states containing two photons and missing energy [2, 3].

In this paper we take a detailed look at the low-energy spectrum of the simplest models with gauge-mediated supersymmetry breaking. We begin by describing the models, elaborating on the issues associated with electroweak symmetry breaking. We use two-loop renormalization group equations and the full one-loop threshold corrections to determine the parameter space which gives rise to consistent radiative electroweak symmetry breaking. We find the Higgs boson and superpartner masses to the same level of accuracy. We comment on how our results are affected by higher-order messenger-sector corrections. We compare the spectra of the simplest gauge-mediated models with those from the minimal supergravity-inspired model. Finally, we identify next-to-lightest supersymmetric particle and compute its lifetime and branching ratios across the allowed parameter space.

## 2 Electroweak symmetry breaking

In models of gauge-mediated supersymmetry breaking, the  $\text{SU}(3) \times \text{SU}(2) \times \text{U}(1)$  gauge interactions of “messenger” fields communicate supersymmetry breaking from a hidden sector to the fields of the visible world. In the simplest models [1], the messenger sector contains a set of vector-like fields,  $M_i$  and  $\overline{M}_i$ , coupled to a standard-model singlet,  $S$ , through the superpotential interaction

$$W_{\text{messenger}} = \lambda_i S M_i \overline{M}_i . \quad (1)$$

The lowest and  $F$ -components of the singlet superfield  $S$  acquire vevs through their interactions with the hidden fields.

To maintain the near unification of the standard-model gauge couplings, we will take the fields  $M_i$  and  $\overline{M}_i$  to transform in complete SU(5) representations. In the same spirit, we will also require that the gauge couplings remain perturbative up to the unification scale. This implies that we can consider at most four  $5 + \overline{5}$  pairs, or one  $10 + \overline{10}$  and one  $5 + \overline{5}$  pair.

In what follows we will take the fields  $M_i$  and  $\overline{M}_i$  to lie in  $(n_5, n_{10})$   $5 + \overline{5}$  and  $10 + \overline{10}$  SU(5) representations. We will assume that these fields couple to the singlet  $S$  through a single Yukawa coupling  $\lambda$  at the unification scale. (See ref. [4] for a discussion of variations.) Below that scale, the SU(5) representations split apart, and the Yukawa couplings evolve according to their own renormalization group equations [5]. We will ignore this splitting in most of what follows; we will remark on it briefly in sect. 3.

The lowest and  $F$  components of the superfield  $S$  acquire vevs through interactions with the sector which dynamically breaks supersymmetry. These vevs induce masses and mixings for the messenger fields. The messenger fermions gain mass  $M = \lambda \langle S \rangle$ , while the messenger scalars obtain the mass matrix

$$\begin{pmatrix} M^2 & \lambda \langle F_S \rangle \\ \lambda \langle F_S \rangle & M^2 \end{pmatrix}. \quad (2)$$

From this point on, we omit the brackets which denote the vevs.

Following the philosophy of dynamical models, we will assume that the standard-model  $\mu$ -term and all soft supersymmetry-breaking terms arise dynamically. For the case at hand, the messenger fields transmit the supersymmetry breaking to the visible sector through loop diagrams which contain insertions of the  $S$  superfield. Such diagrams induce weak-scale masses for the gauginos and scalars of the minimal supersymmetric standard model. However, they cannot give sizable values for the soft supersymmetry-breaking  $A$  parameters. In what follows, we shall set all  $A$ -terms to zero at the messenger scale.

The messenger fields induce the following gaugino

$$\tilde{M}_i(M) = (n_5 + 3n_{10}) g \left( \frac{\Lambda}{M} \right) \frac{\alpha_i(M)}{4\pi} \Lambda \quad (3)$$

and scalar

$$\tilde{m}^2(M) = 2(n_5 + 3n_{10}) f \left( \frac{\Lambda}{M} \right) \sum_{i=1}^3 k_i C_i \left( \frac{\alpha_i(M)}{4\pi} \right)^2 \Lambda^2 \quad (4)$$

masses at the scale  $M$ , where  $\Lambda = F_S/S$  and  $k_i = 1, 1, 3/5$  for SU(3), SU(2), and U(1), respectively. The  $C_i$  are zero for gauge singlets, and  $4/3, 3/4$ , and  $Y^2$  for the fundamental representations of SU(3), SU(2), and U(1). Here  $Y = Q - I_3$  denotes the usual hypercharge and we use the grand unification normalization for  $\alpha_1$ . Because a pair of  $10 + \overline{10}$  fields contributes to the soft masses as if  $n_5 = 3$ , we will set  $n_{10} = 0$  and only consider changes in  $n_5$ .

The messenger-scale threshold functions [4, 6]

$$g(x) = \frac{1+x}{x^2} \log(1+x) + (x \rightarrow -x), \quad (5)$$

$$f(x) = \frac{1+x}{x^2} \left[ \log(1+x) - 2\text{Li}_2 \left( \frac{x}{1+x} \right) + \frac{1}{2} \text{Li}_2 \left( \frac{2x}{1+x} \right) \right] + (x \rightarrow -x), \quad (6)$$

have the property that  $g(x)$ ,  $f(x) \rightarrow 1$  as  $x \rightarrow 0$ , or  $\Lambda \ll M$ . In this limit, the expressions (3) and (4) take the characteristic simple forms [1] that are often associated with gauge-mediated models.

The region  $\Lambda \rightarrow M$  corresponds to  $x \rightarrow 1$ , where  $g(1) \simeq 1.4$  and  $f(1) \simeq 0.7$ . We must exclude the limit  $M = \Lambda$  because it gives rise to a massless messenger scalar. For the purposes of this paper, we restrict ourselves to the region  $x < 0.97$ , or  $M/\Lambda > 1.03$ . This corresponds to an upper limit on the fine tuning of the messenger masses; it is obtained by requiring that the average scalar mass-squared be less than 30 times the light scalar mass-squared.

Equations (3) and (4) serve as boundary conditions for the renormalization group equations at the messenger scale,  $M$ . They give rise to rather generic predictions for the soft supersymmetry-breaking gaugino and scalar masses. In contrast, the boundary conditions for  $B(M)$  and  $\mu(M)$  are more model-dependent.<sup>1</sup> New interactions are necessary to induce these terms because they violate a Peccei-Quinn symmetry in the effective action [7, 8]. The new interactions can give rise to additional contributions to the scalar masses beyond those in (4). In particular, they can give additional contributions to the Higgs masses,  $m_{H_1}^2$  and  $m_{H_2}^2$ .

In this paper, we will not commit ourselves to a particular model for  $B(M)$  and  $\mu(M)$ . Instead, we will take a more phenomenological approach and treat them as free parameters. We will, however, assume that the soft Higgs masses  $m_{H_1}^2$  and  $m_{H_2}^2$  are given by eq. (4). We will also require that electroweak symmetry be radiatively broken.

Our approach is as follows. We start at the messenger scale,  $M$ , and fix the boundary conditions (3) and (4). We use the two-loop renormalization group equations to run the soft masses down to the squark mass scale,  $M_{\tilde{q}} \simeq \sqrt{n_5} \Lambda/90$ , where we impose electroweak symmetry breaking and calculate the supersymmetric mass spectrum. At the squark scale, we consistently include all one-loop weak-scale threshold corrections. These corrections play an important role in determining  $B(M_{\tilde{q}})$  and  $\mu(M_{\tilde{q}})$ . We then run  $B$ ,  $\mu$  and the gauge and Yukawa couplings back to the messenger scale. We repeat the procedure until we find a self-consistent solution for  $B(M)$  and  $\mu(M)$  in terms of the  $Z$ -boson pole mass,  $M_Z$ , and the ratio of Higgs vacuum expectation values,  $\tan \beta$ . (We take the top- and bottom-quark pole masses to be  $m_t = 175$  GeV,  $m_b = 4.9$  GeV, and the  $\overline{\text{MS}}$  value of the strong coupling to be  $\alpha_s(M_Z) = 0.118$ .)

We note that there are messenger-scale threshold corrections which we do not take into account, even though they are formally the same order as the weak-scale threshold corrections. We choose to ignore these corrections because they are model dependent. We will, however, estimate their importance by determining the sensitivity of our results to small changes in the messenger-scale boundary conditions.

With these assumptions, the parameter space of this minimal model is described by  $\tan \beta$ , the scale  $\Lambda$ , the messenger scale  $M$ , along with  $n_5$ , the effective number of  $5 + \bar{5}$  messenger fields, and the sign of  $\mu$ . We will first set  $n_5 = 1$  and  $M = 2\Lambda$ . This leaves a two-dimensional parameter space,  $(\Lambda, \tan \beta)$ , for each sign of  $\mu$ .

In Fig. 1 we show our results for  $B(M)/\mu(M)$  and  $\mu(M)$  in the  $(\Lambda, \tan \beta)$  plane. We see that consistent electroweak symmetry breaking requires  $|\mu(M)|$  to be in the range from 150

---

<sup>1</sup>The parameter  $\mu$  is the standard supersymmetric Higgsino mass;  $B$  is the dimension-two soft mass that is often denoted  $B\mu$  in supergravity-inspired models.

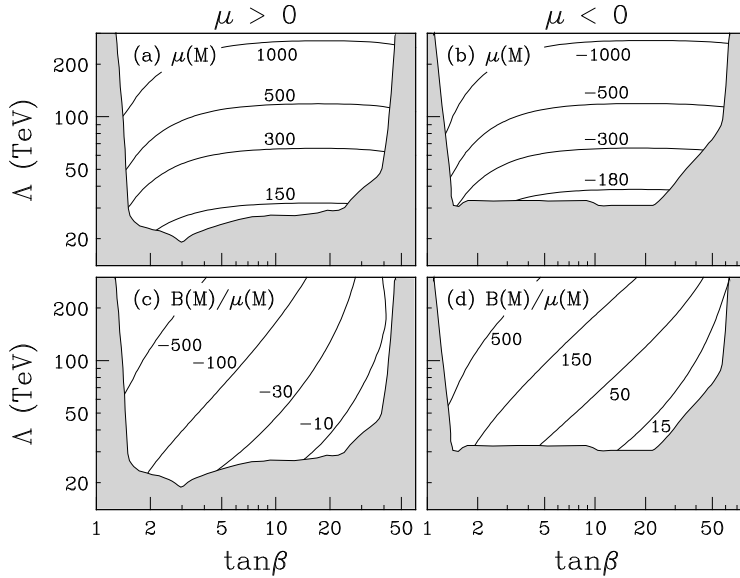


Figure 1: Contours of  $\mu(M)$  and  $B(M)/\mu(M)$  in the  $\Lambda$ ,  $\tan\beta$  plane, with  $n_5 = 1$  and  $M/\Lambda = 2$ . The contours are labeled in GeV.

GeV for small  $\Lambda$  to over 1 TeV for large  $\Lambda$ . We also find that  $B(M)/\mu(M)$  ranges from near zero, at the largest values of  $\tan\beta$ , to  $\gtrsim 500$  GeV at small  $\tan\beta$ . We do not consider  $\Lambda > 300$  TeV because of fine tuning considerations.

Various constraints exclude the border regions in Fig. 1 (and the remaining contour plots). The region of small  $\tan\beta$  is excluded because the top Yukawa coupling diverges below the unification scale. This is not necessarily fatal, but since we wish to preserve perturbative grand unification, we require  $\lambda_t(M_{\text{GUT}}) < 3.5$ . The region of very large  $\tan\beta$  is excluded because electroweak symmetry is not broken. Typically, we find  $m_A^2 < 0$  in the large  $\tan\beta$  region.

The region at small  $\Lambda$  is excluded because of the usual experimental bounds on the masses of supersymmetric particles, most notably  $m_{\tilde{\chi}^+} < 65$  GeV. (We use the bounds listed in Ref. [13].) These bounds hold when the LSP is the lightest neutralino and is stable. They also hold in gauge-mediated models when the NLSP is  $\tilde{\chi}_1^0$  and it decays outside the detector. In sect. 4 we delineate the regions of the parameter space where this applies. If the NLSP decays inside the detector, the collider bounds are stronger because the decay modes (e.g.  $\tilde{\chi}_1^0 \tilde{\chi}_1^0 \rightarrow \gamma\gamma + \text{missing energy}$ ) have much smaller backgrounds [2].

In Fig. 2 we plot the scale dependence of  $B(M)/\mu(M)$  and  $\mu(M)$  to illustrate the importance of the weak-scale threshold corrections. We see that our results, which consistently incorporate the weak-scale thresholds, have significantly less scale dependence than they would if the corrections were ignored. Furthermore, we see that the threshold corrections are especially important at large  $\tan\beta$ , where  $B(M)$  is small. The largest threshold corrections arise from squark loops, so the threshold corrections are smallest in the vicinity of the squark scale,  $M_{\tilde{q}} = \sqrt{n_5} \Lambda/90$ . Indeed, in Figs. 2(a-c) we see that the tree-level result is nearly equal to the full result at the scale  $M_{\tilde{q}}/2$ . If we vary the scale over a reasonable range, e.g.  $M_{\tilde{q}}/2$  to  $2M_{\tilde{q}}$ , we find that the weak-scale threshold corrections (between 5% and 15%) are generally larger than the corrections from the two-loop evolution (about 2%), as might be expected because

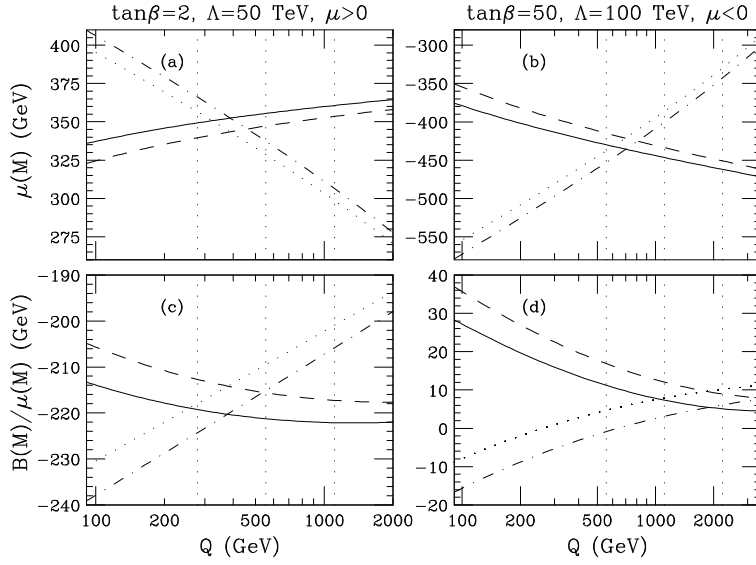


Figure 2: The parameters  $\mu(M)$  and  $B(M)/\mu(M)$  as a function of the scale,  $Q$ , where the renormalization group evolution is stopped and electroweak symmetry breaking is imposed. The dotted (dot-dashed) lines include the one-loop (two-loop) evolution equations, but no weak-scale thresholds. The dashed (solid) lines include the one-loop (two-loop) evolution equations, plus the full set of one-loop weak-scale thresholds. The dotted vertical lines on each plot denote the squark scales  $M_{\tilde{q}}/2$ ,  $M_{\tilde{q}}$  and  $2M_{\tilde{q}}$ .

of the relatively small amount of running.

The region  $B(M) \simeq 0$  is of considerable phenomenological interest [8, 9]. For instance, models where  $B(M) \simeq 0$  give rise to large  $\tan\beta$  without fine tuning [8]. Furthermore, since the  $A$ -terms are also small at the scale  $M$ , such models have a naturally small neutron electric dipole moment [8]. Indeed, only the small  $\mathcal{O}(\alpha M_2/\pi)$  starting values of  $A(M)$  and  $B(M)/\mu(M)$  can contribute to the neutron EDM. The pieces of  $A$  and  $B$  which are generated by the renormalization group,  $A_{RG}$  and  $B_{RG}$ , do not contribute because they are proportional to  $M_2$  and  $\mu M_2$ , so the invariant CP-violating phases [12]  $\arg(A_{RG}^* M_2)$  and  $\arg(B_{RG}^* \mu M_2)$  vanish.

The region of  $B(M) \simeq 0$  is associated with the region of large  $\tan\beta$ . At tree level, we have

$$B = \frac{m_{H_1}^2 - m_{H_2}^2}{\tan\beta - \cot\beta} - \frac{M_Z^2}{\tan\beta + \cot\beta}, \quad (7)$$

which implies that  $B$  decreases as  $\tan\beta$  increases. From Fig. 1 we find, for  $n_5 = 1$  and  $M = 2\Lambda$ , that  $B(M)$  is small (but non-zero) along the excluded region at large  $\tan\beta$ . (Our results should be contrasted with those of ref. [9], which do not include one-loop thresholds. The authors of ref. [9] find  $B(M) = 0$  for  $\tan\beta \simeq 20$  and  $\mu < 0$ .)

Until now we have restricted our attention to the simple case where  $M/\Lambda = 2$ . In principle,  $M/\Lambda$  can be much larger. A large hierarchy  $M \gg \Lambda$  can arise from a small Yukawa coupling or from loop factors [10]. An upper bound on this splitting can be obtained from the cosmological constraint that the gravitino relic density not overclose the universe. In the usual inflationary scenario, this translates into an upper bound on the gravitino mass of about 1 keV [14]. If

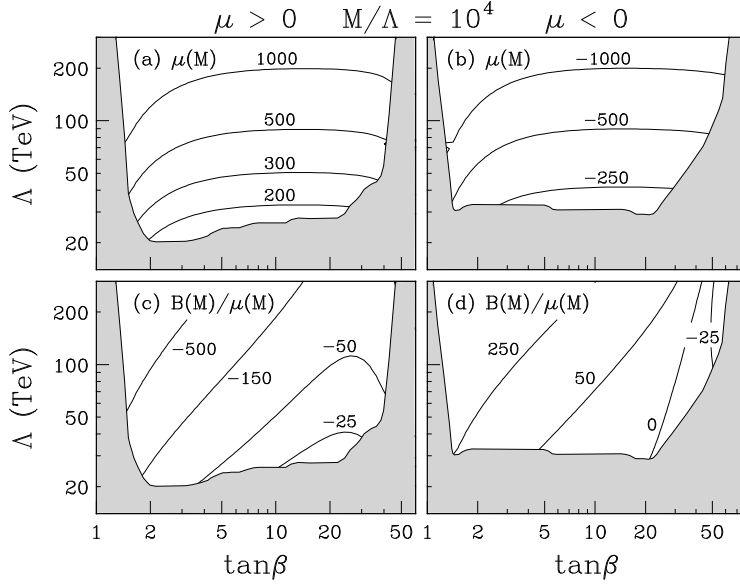


Figure 3: The same as Fig. 1, with  $M/\Lambda = 10^4$  and  $n_5 = 1$ . The magnitude of  $\mu(M)$  is increased relative to that of Fig. 1.

we assume that the singlet  $F$ -term is of the same order of magnitude as the largest  $F$ -term in the theory, we have

$$m_{\tilde{G}} \simeq \frac{F_S}{M_P} = \left( \frac{M}{\Lambda} \right) \frac{\Lambda^2}{M_P}, \quad (8)$$

Setting  $\Lambda = 30$  TeV, we find that  $m_{\tilde{G}} \simeq 1$  keV if  $M/\Lambda \simeq 10^4$ . Hence we will not consider values of  $M/\Lambda$  larger than  $10^4$ .

As we increase  $M$  for a fixed  $\Lambda$ , there is more renormalization group evolution, so there are larger splittings between the soft Higgs masses. These, in turn, give somewhat larger values of  $\mu(M)$ . We show this in Figs. 3(a-b), where we plot contours of  $\mu(M)$  in the  $(\Lambda, \tan \beta)$  plane, for  $n_5 = 1$  and  $M/\Lambda = 10^4$ . We see that the values of  $\mu(M)$  are slightly larger than those in Fig. 1. The situation for  $B(M)$  is more subtle because the region  $B(M) \simeq 0$  is sensitive to additive radiative corrections. In Figs. 3(c-d) we show our results for  $M/\Lambda = 10^4$ . We find that  $B(M) = 0$  occurs for  $\mu < 0$  with  $\tan \beta \simeq 20$  to  $40$ , depending on  $\Lambda$ . For smaller  $M/\Lambda$ , the  $B(M) = 0$  contour in Fig. 3(d) moves to the right, to larger values of  $\tan \beta$ .

In Fig. 4 we plot the pole mass of the lightest Higgs boson,  $m_h$ , and of the CP-odd Higgs boson,  $m_A$ , in the  $(\Lambda, \tan \beta)$  plane, for  $M/\Lambda = 2$  and  $10^4$ . We see that  $m_h \lesssim 130$  GeV, and that  $m_A$  is nearly always larger than 200 GeV. For such large values of  $m_A$ , all three heavy Higgs bosons are nearly degenerate in mass.

The above results depend sensitively on  $n_5$ , the number of  $5 + \bar{5}$  pairs. In Fig. 5 we show, for  $M = 2\Lambda$  and  $10^4$ , contour plots with  $n_5 = 2, 3$  and  $4$ . The change in the parameter  $\mu(M)$  is dominated by the change in the scalar masses. Indeed, we find  $\mu(M)/\Lambda \propto \sqrt{n_5}$ , as expected from eq. (4). The ratio  $B(M)/\mu(M)$  obeys the same scaling at small  $\tan \beta$ . At large  $\tan \beta$ , however, the change in  $B(M)$  is more complicated. This is the region where  $B(M)$  is small, so its value depends sensitively on radiative corrections. For  $\mu > 0$ , there is a line in parameter space where  $B(M) = 0$  at large  $\Lambda$ . For  $\mu < 0$ , however,  $B(M)$  is never zero. We find  $B(M)/\mu(M) > 10$  GeV for  $n_5 = 4$ .

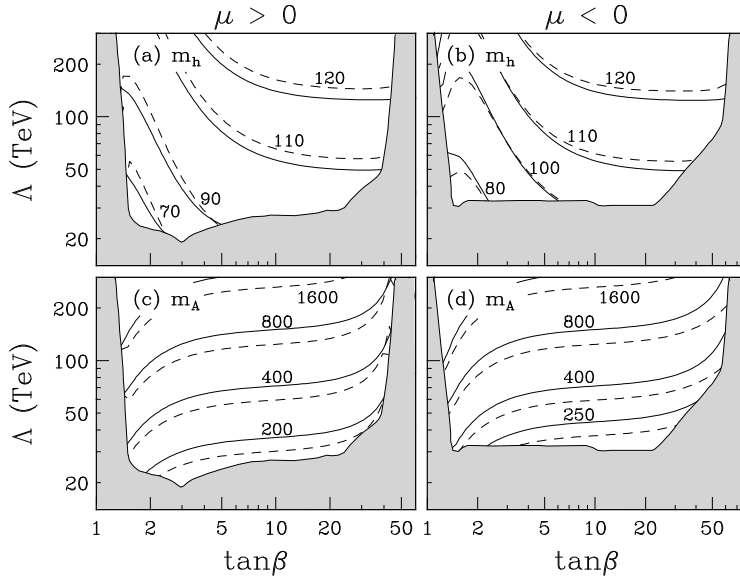


Figure 4: Figures (a) and (b) show contours of the light CP-even Higgs-boson mass,  $m_h$ , in GeV, while Figs. (c) and (d) show the CP-odd Higgs-boson mass,  $m_A$ , in GeV. We set  $n_5 = 1$ , and the solid (dashed) lines correspond to  $M/\Lambda = 2$  ( $10^4$ ).

The results presented here have varying degrees of sensitivity to the input parameters. We illustrate this sensitivity by computing the changes in  $B(M)/\mu(M)$  and  $\mu(M)$ . We first vary the quark masses,  $m_b = 4.9 \pm 0.5$  GeV and  $m_t = 175 \pm 5$  GeV, and find a shift  $\Delta|B/\mu| \lesssim 10$  GeV and  $|\Delta\mu/\mu| \lesssim 7\%$  in the region  $B(M) \simeq 0$ . To estimate the sensitivity to messenger-scale threshold corrections, we randomly vary the soft masses at the messenger scale by 5%. In the region  $B(M) \simeq 0$ , we find shifts in  $B(M)/\mu(M)$  of up to 10 GeV, and changes in  $\mu$  of order 5%.

### 3 The spectrum

In this section we find the masses of the supersymmetric particles that arise in the gauge-mediated scheme. We examine how the spectrum depends on the parameter space, and comment on the sensitivity to low- and high-energy threshold corrections. As above, we follow a self-consistent procedure. We start with the masses (3) and (4) at the messenger scale,  $M$ . We then use the two-loop renormalization group equations to run these masses to the squark scale,  $M_{\tilde{q}} = \sqrt{n_5} \Lambda/90$ . At that scale we apply the one-loop threshold corrections and impose electroweak symmetry breaking. We then calculate the superpartner masses, and run the gauge couplings back to the messenger scale. We iterate this procedure to determine the consistent one-loop superpartner pole masses. The weak-scale threshold corrections for all the superpartner masses are contained in ref. [13].

Figure 6 shows the spectrum in the canonical case where the messenger scale  $M$  is equal to  $2\Lambda$ . We plot the various masses against the mass of the lightest neutralino,  $\tilde{\chi}_1^0$ . The first point to note is that, for  $m_{\tilde{\chi}_1^0} \gtrsim 100$  GeV, most of the curves are rather flat. This simply reflects the fact that most of the masses, including  $m_{\tilde{\chi}_1^0}$ , scale with  $\Lambda$ . The only exceptions are the light Higgs,  $h$ , whose mass is determined by radiative corrections (the correction to its



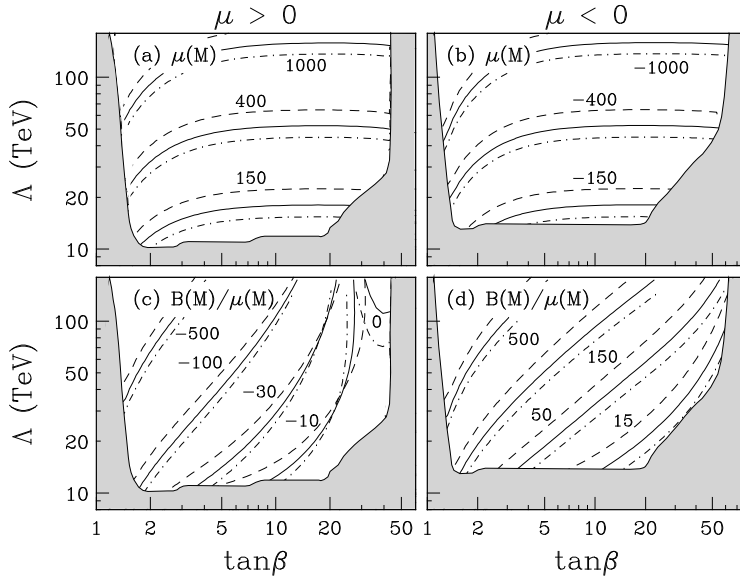


Figure 5: The same as Fig. 1 for varying  $n_5$ . The dashed, solid and dot-dashed lines correspond to  $n_5 = 2, 3, 4$ , respectively. The values of  $\mu(M)$  and  $B(M)/\mu(M)$  scale like  $\sqrt{n_5}$  for a fixed value of  $\Lambda$ , except for  $B(M) \simeq 0$ , where radiative corrections are important.

mass-squared grows like  $\ln \Lambda$ ), and the light tau slepton, whose mass is significantly affected by left-right mixing.

Because of the large mixing in the tau slepton mass matrix, the light tau slepton mass is especially sensitive to radiative corrections. The one-loop self-energy correction is typically less than  $\mathcal{O}(3\%)$  (see Ref. [13]). However, for large  $\tan \beta$ , the large threshold corrections to  $\mu$  (see Fig. 2) induce a significant shift in the light tau slepton mass. In Fig. 7(a) we plot the light tau slepton mass versus  $\tan \beta$ . We show the one-loop and tree-level results, for various choices of the renormalization scale,  $Q$ . At large  $\tan \beta$ , the corrections can be of order 30%. In Fig. 7(b) we show the scale dependence of the one-loop and tree-level tau slepton masses, as well as the effect of the two-loop renormalization group evolution. The weak-scale threshold corrections significantly reduce the scale dependence of the pole mass. As expected, the two-loop renormalization group effects are small because of the small amount of running.

The tau slepton mass matrix should be contrasted with those of the top and bottom squarks. These matrices can also have substantial mixing, but the mixing does not significantly change the mass eigenvalues. This implies that the masses of the light top and bottom squarks cannot be much less than the masses of the other squarks. Indeed, we find that the mass of the light top squark is typically 10 to 20% less than that of the other squarks, although it can be as much as 35% less at the smallest values of  $\tan \beta$ . Similarly, the light bottom squark mass is usually 0 to 10% less than that of the other squarks, but it can be as much as 25% less at the largest values of  $\tan \beta$ .

In Fig. 6 we see that for  $m_{\tilde{\chi}_1^0} \lesssim 100$  GeV, the curves leave their linear trajectories, especially for  $\tan \beta = 2$  with  $\mu$  negative. This is because for small  $m_{\tilde{\chi}_1^0}$ , the mixing in the neutralino mass matrix become increasingly important, so the  $\tilde{\chi}_1^0$  mass no longer scales with  $\Lambda$ . This is illustrated in Fig. 8, where we show the  $\tilde{\chi}_1^0$  mass as a function of  $\Lambda$ .

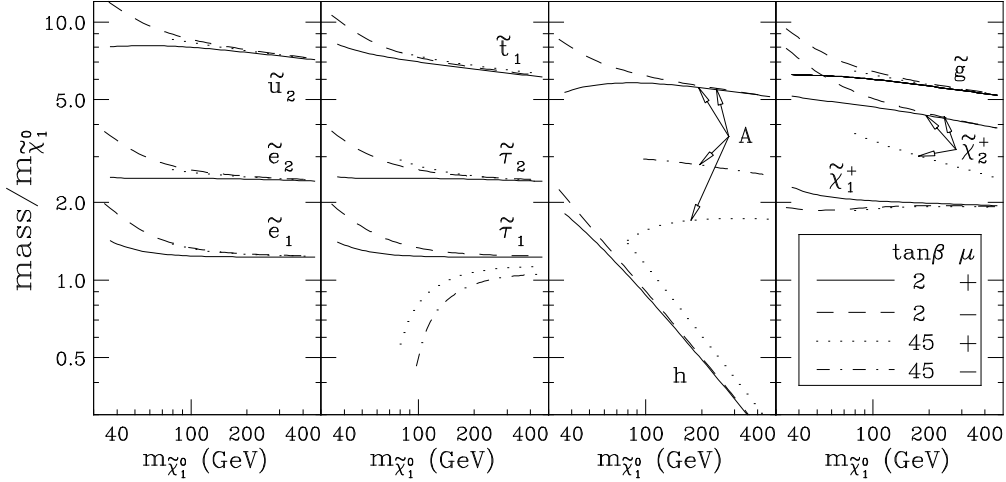


Figure 6: The ratio of various superpartner masses to  $m_{\tilde{\chi}_1^0}$ , versus  $m_{\tilde{\chi}_1^0}$ , for  $M = 2\Lambda$  and  $n_5 = 1$ . The different lines for each particle correspond to the cases of small/large  $\tan\beta$  and positive/negative  $\mu$ . Except for  $m_A$  and  $m_{\tau_1}$ , the large  $\tan\beta$  curves are essentially independent of the sign of  $\mu$ .

The previous spectra were all computed with  $M = 2\Lambda$ . If  $M$  is increased with respect to  $\Lambda$ , the masses change in two ways. First, the initial conditions are different because the masses at the scale  $M$  depend on  $\alpha_i(M)$ . Second, more running is needed to reach the squark scale,  $M_{\tilde{q}}$ .

These effects almost cancel for the gaugino masses because the gaugino masses obey the same one-loop renormalization group equations as the gauge couplings. They do, however, change the scalar masses. For squarks, the two effects work in opposite directions. It turns out that for  $n_5 = 1$  the change in the boundary conditions is more important, so the squark masses are reduced. For  $n_5 = 3$  the two effects largely cancel. For sleptons, the effects work in the same direction, and give a slight increase in the slepton masses. The shifts in the scalar masses are illustrated in Fig. 9. The small changes indicate that it is safe to ignore any factor of two or three change in the messenger quarks scale with respect to the messenger lepton scale, such as might be induced by renormalization group evolution of the messenger Yukawa coupling  $\lambda$ .

Figure 9 also illustrates the importance of the threshold functions  $f(x)$  and  $g(x)$ . In the region  $1.03 \lesssim M/\Lambda \lesssim 2$  the threshold functions lead to significant increases in the gaugino masses, and to small decreases in the scalar masses, relative to the case when  $M/\Lambda \gtrsim 2$ . The threshold corrections are so important that the light tau slepton becomes the NLSP for  $M$  near  $\Lambda$ .

In Fig. 9 we also show the effect of increasing  $n_5$  from 1 to 3. The gaugino masses scale like  $n_5$ , while the scalar masses go like  $\sqrt{n_5}$ . Because of this fact, for the case of a  $10 + \overline{10}$  pair of messenger fields ( $n_5 = 3$ ), the light tau slepton is the NLSP over most of the parameter space. We discuss this in more detail in the next section.

Note that the squark masses are light enough that they will be produced in the next generation of colliders over most of the parameter space.

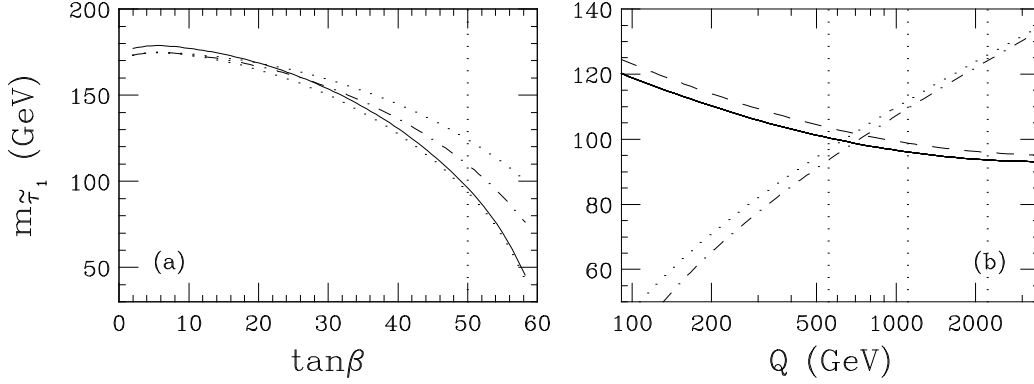


Figure 7: (a) The light tau slepton mass versus  $\tan\beta$ , for  $n_5 = 1$ ,  $\Lambda = 100$  TeV,  $M = 2\Lambda$ , and  $\mu < 0$ . The one-loop result (solid) and tree-level results for  $Q = M_{\tilde{q}}/2$ ,  $M_{\tilde{q}}$ , and  $M_{\tilde{q}}$  are shown. The tree-level curve for  $Q = M_{\tilde{q}}/2$  is closest to the full result. (b) The scale dependence of the tau slepton mass for the same parameters, with  $\tan\beta = 50$ . The full result (solid) is contrasted with the tree-level result (dot-dashed). The corresponding curves obtained using one-loop renormalization group evolution are shown (dashed, dotted).

As above, we can estimate the sensitivity of the supersymmetric spectrum to messenger-scale thresholds by varying the soft masses at the messenger scale by 5%. We find that most of the pole masses vary by about 5%, except for the light Higgs, which varies by  $\lesssim 1\%$ , and the top and bottom squarks, which change by up to 10%. The light tau slepton mass varies by up to 15%, except at a few exceptional points, where the variation can be as large as 70%. This large sensitivity in the tau slepton mass occurs at large  $\tan\beta$ , in the region where it is potentially the NLSP.

We will conclude this section by contrasting the predictions of the gauge-mediated models with the predictions of the minimal supergravity model. At the unification scale, the inputs to the supergravity model are a universal scalar mass,  $M_0$ , a common gaugino mass,  $M_{1/2}$ , and a trilinear scalar coupling  $A_0$ . As in the gauge-mediated model, radiative breaking of electroweak symmetry breaking is imposed.

In general, the two models predict qualitatively different spectra. The supergravity model includes separate scales for the gauginos and the scalars, so the scalars can be much heavier than the gauginos. The gauge-mediated models have only one scale, so the ratios of the gaugino to the scalar masses are more or less fixed. We illustrate this in Fig. 10(a), where we show the ratio of the (first or second generation) squark mass to the gluino mass in the two models.<sup>2</sup> In the supergravity case, this ratio varies from about 0.9 to 5. For gauge-mediated models, the ratio depends on  $n_5$ . For  $n_5 = 1$ , the squarks are 20 to 40% heavier than the gauginos, while for  $n_5 = 4$  the squarks are about 5 to 10% lighter. (These numbers and the bands on the figure ignore the region  $M \lesssim 2\Lambda$ , where the ratio  $m_{\tilde{q}}/m_{\tilde{g}}$  falls by 20%.) Note that gauge-mediated models with  $n_5 = 4$  predict the same ratio of squark to gluino mass as the supergravity models with  $M_0 \lesssim M_{1/2}$ .

In the region where the two models predict the same gluino and squark masses, they do

<sup>2</sup>The supergravity scatter plots were generated as in Ref. [13].

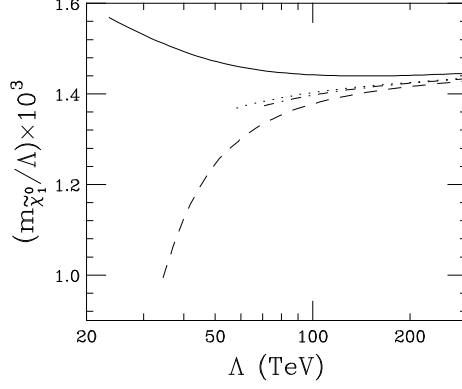


Figure 8: The ratio  $m_{\tilde{\chi}_1^0}/\Lambda$  versus  $\Lambda$ , for the same choice of parameters as in Fig. 6.

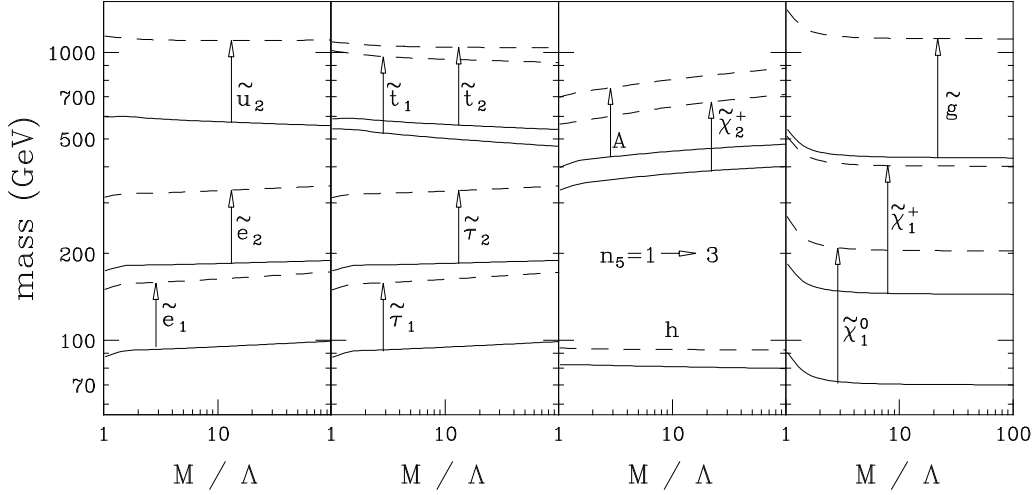


Figure 9: Various sparticle masses versus the ratio  $M/\Lambda$ , for  $\Lambda = 50$  TeV,  $\tan \beta = 2$  and  $\mu > 0$ . The solid (dashed) lines correspond to  $n_5 = 1$  ( $n_5 = 3$ ).

not typically predict the same slepton masses. We illustrate this in Fig. 10(b), where we show a supergravity scatter plot of the ratio of the left-handed to the right-handed selectron mass, versus  $M_0/M_{1/2}$ . On the scatter plot we superimpose the prediction of the gauge-mediated model, for  $n_5 = 4$ , divided up into regions of small and large right-handed selectron mass ( $m_{\tilde{e}_R} < M_Z$  and  $m_{\tilde{e}_R} > M_Z$ ). In the small  $m_{\tilde{e}_R}$  region the  $D$ -term contributions to the slepton masses become important. These  $D$ -term contributions can make the selectron ratios coincide with the supergravity model prediction in the region  $M_0 \ll M_{1/2}$  if  $\tan \beta$  is less than 3 in supergravity model and larger than 5 in the gauge-mediated model.

If we go even further, we find that the two models can predict the same gluino, squark, charged slepton and light chargino masses. We give an example in Table 1. This table lists the spectra for the supergravity model parameters  $\tan \beta = 2.1$ ,  $M_0 = 5$  GeV,  $M_{1/2} = 145$  GeV,  $A_0 = 686$  GeV, and  $\mu < 0$ , and for the gauge-mediated model parameters  $\tan \beta = 14$ ,  $\Lambda = 11$  TeV,  $M/\Lambda = 3716$ ,  $n_5 = 4$  and  $\mu < 0$ . The overlap can occur only for small selectron

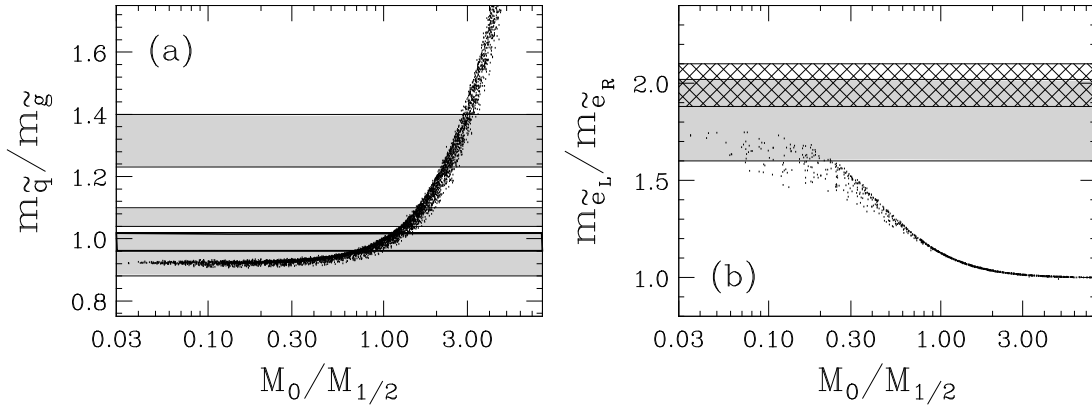


Figure 10: (a) The ratio of the (first or second generation) squark mass to the gluino mass in the supergravity-inspired (dots) and gauge-mediated models (bands). The four bands in the gauge-mediated case correspond to  $n_5 = 1, 2, 3, 4$ . The largest ratio (uppermost band) is for  $n_5 = 1$ . (b) The ratio of the left-handed to the right-handed selectron mass in the two models. The scatter plot shows the supergravity model prediction. The bands mark, in the gauge-mediated model with  $n_5 = 4$ , the regions where  $m_{\tilde{e}_R} < M_Z$  (grey) and  $m_{\tilde{e}_R} > M_Z$  (hatched).

and  $\tilde{\chi}_1^0$  masses, where the slepton  $D$ -terms and the gaugino/Higgsino mixing come into play.

Table 1 also illustrates that the models differ in their predictions for other observables. If we scan over the parameter spaces of the two models and match the gluino masses to 8%, and the light chargino and (first and second generation) squark and selectron masses to 2%, we find that the two models predict different values of  $\tan\beta$ , as well as significantly different masses for the neutralinos, the sneutrinos, the heavy chargino and the light Higgs boson. They also predict different values for the Higgs parameters  $\mu$  and  $m_A$ , and, typically, different masses for the third-generation squarks and sleptons.

We illustrate these differences in Fig. 11, where we show scatter plots of the values of  $\tan\beta$ ,  $m_h$ ,  $m_A$ , and  $m_{\tilde{\chi}_2^+}$  in the two models. We see that the models are clearly distinguished. Note that since both models have essentially one scale there is a strong correlation between the heavy Higgs and Higgsino masses. (The two scales are  $\Lambda$  and  $M_{1/2}$ , since  $M_0 \simeq 0$ .) We conclude that it is possible, but not probable, that measurements of the gluino, squark, slepton and light chargino masses may not be enough to discriminate the gauge-mediated from the supergravity model. However, additional measurements would easily rule out one (or both) of the models.

## 4 Properties of the NLSP

In the preceding section, we saw that the NLSP is either the light tau slepton,  $\tilde{\tau}_1$ , or the lightest neutralino,  $\tilde{\chi}_1^0$ . Over most of the parameter space, the number of  $5 + \bar{5}$  pairs determines the NLSP. For  $n_5 = 1$ , the  $\tilde{\chi}_1^0$  tends to be the NLSP. For larger  $n_5$ , the balance tips towards the  $\tilde{\tau}_1$  because as  $n_5$  increases, the scalar masses increase less than their gaugino counterparts.

In Fig. 12 we plot contours of  $m_{\tilde{\chi}_1^0} = m_{\tilde{\tau}_1}$  in the  $(m_{\tilde{\chi}_1^0}, \tan\beta)$  plane, for each value of  $n_5$

$\Delta m/m < 2\%$			$\Delta m/m > 2\%$			
	GMSB	SUGRA		GMSB	SUGRA	% diff.
$m_{\tilde{g}}$	361	366	$m_{\tilde{\nu}_e}$	72	85	-19
$m_{\tilde{u}_L}$	336	337	$m_{\tilde{t}_R}$	281	235	16
$m_{\tilde{u}_R}$	328	329	$m_{\tilde{b}_R}$	330	322	3
$m_{\tilde{d}_L}$	345	343	$m_{\tilde{\tau}_L}$	115	105	8
$m_{\tilde{d}_R}$	330	329	$m_{\tilde{\tau}_R}$	46	63	-37
$m_{\tilde{e}_L}$	107	106	$m_{\tilde{\nu}_\tau}$	71	85	-19
$m_{\tilde{e}_R}$	64	64	$m_{\tilde{\chi}_1^0}$	49	45	9
$m_{\tilde{t}_L}$	382	382	$m_{\tilde{\chi}_3^0}$	175	276	-58
$m_{\tilde{b}_L}$	309	304	$m_{\tilde{\chi}_4^0}$	210	307	-46
$m_{\tilde{\chi}_1^+}$	83	82	$m_{\tilde{\chi}_2^+}$	212	303	-43
$m_{\tilde{\chi}_2^0}$	87	87	$m_h$	104	77	26
			$m_A$	170	318	-87

Table 1: Comparison of the spectra of the gauge-mediated (GMSB) and supergravity-inspired (SUGRA) models. The masses are in units of GeV.

between 1 and 4. Each subfigure contains four contours, two for each sign of  $\mu$ , and two for  $M/\Lambda = 2$  and  $10^4$ . We see that for  $n_5 = 1$ , the neutralino is the NLSP, except for small regions at large  $\tan\beta \gtrsim 25$  and small  $m_{\tilde{\chi}_1^0}$ . For  $n_5 = 2$  and  $M/\Lambda = 10^4$ ,  $\tilde{\chi}_1^0$  is the NLSP for  $\tan\beta \lesssim 20 - 30$ . For  $n_5 = 2$  and  $M/\Lambda = 2$ , the light tau slepton is the NLSP over most of the parameter space, as it is for  $n_5 = 3$  or 4 and arbitrary  $M/\Lambda$ . For  $n_5 > 2$ , the neutralino is the NLSP at very small  $m_{\tilde{\chi}_1^0} \lesssim 100$  GeV.

These results are subject to significant uncertainties from the unknown messenger-scale thresholds. In particular, the line where  $m_{\tilde{\chi}_1^0} = m_{\tilde{\tau}_1}$  is sensitive to potentially large one-loop corrections to the mass of the light tau slepton. We find that 5% variations in the messenger-scale boundary conditions give rise to a  $m_{\tilde{\chi}_1^0} - m_{\tilde{\tau}_1}$  mass difference of up to 30 GeV in the region where the difference is less than 100 GeV.

The collider phenomenology in gauge-mediated models depends crucially on the nature of the NLSP, especially when it decays inside the detector. The lifetime of the NLSP depends on its mass,  $m$ , and on the ratio  $M/\Lambda$ , as follows,

$$\tau \propto \frac{F_S^2}{m^5} \propto \frac{1}{m} \left( \frac{M}{\Lambda} \right)^2. \quad (9)$$

For the case at hand, where the NLSP is either the  $B$ -ino or the  $\tilde{\tau}_1$ , we can put in the appropriate factors of  $\pi$  and  $\alpha_1$  and write the lifetime in units of meters,

$$c\tau \simeq \left( \frac{100 \text{ GeV}}{m} \right) \left( \frac{M}{\Lambda} \right)^2 \times 10^{-5} \text{ meters}. \quad (10)$$

For  $\beta\gamma = \sqrt{E^2/m^2 - 1} \simeq 1$ , this is the approximate decay length. We see that for  $\beta\gamma \simeq 1$  and  $M/\Lambda \lesssim 100$ , the NLSP will decay inside the detector.

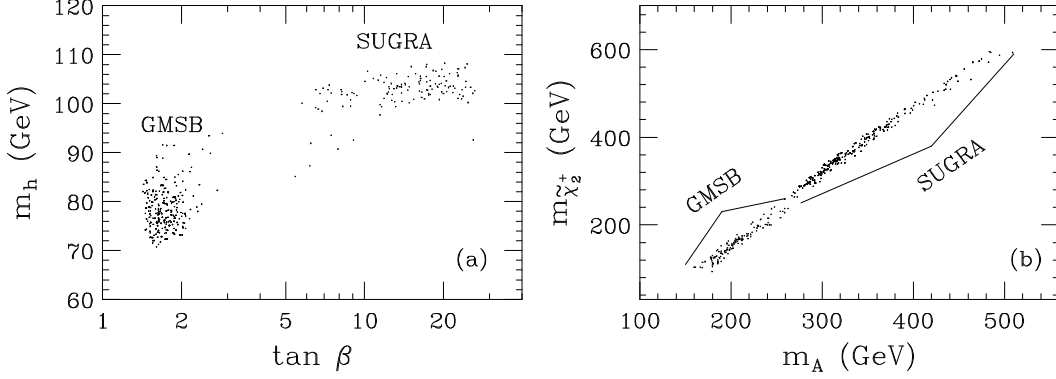


Figure 11: Scatter plots of observables in the regions of parameter space where the gauge-mediated and supergravity models predict the same gluino, squark, slepton and light chargino masses (see text). Figure (a) shows a scatter plot of  $m_h$  versus  $\tan \beta$  in the gauge-mediated (GMSB) and supergravity models (SUGRA). Figure (b) shows  $m_{\tilde{\chi}_2^+}$  versus  $m_A$ .

In Fig. 13 we illustrate the neutralino lifetime in different regions of parameter space. In Fig. 13(a) we plot the lifetime versus the neutralino mass, for  $M/\Lambda = 2$  and 100, with  $n_5 = 1$  and  $\tan \beta = 2$ . In Fig. 13(b) we show a scatter plot of the neutralino lifetime versus  $M/\Lambda$ . The lifetime increases by eight orders of magnitude as we increase  $M/\Lambda$  from 1 to  $10^4$ . In this and the next scatter plot, we vary the parameters  $n_5$  from 1 to 4,  $\Lambda$  from 16 TeV/ $n_5$  to 300 TeV/ $\sqrt{n_5}$ ,  $M/\Lambda$  from 1.03 to  $10^4$ , and  $\tan \beta$  from 1.2 to 70. The latter three variables are sampled on logarithmic measures, subject to the phenomenological constraints discussed in sect. 2.

If the tau slepton is the NLSP, it will decay to a  $\tau$  lepton and a gravitino with a branching fraction that is essentially 100%. The lightest neutralino has many more decay modes because it has Higgsino and gaugino components. The  $\tilde{\chi}_1^0$  can decay to either a Higgs or a gauge boson, plus a gravitino,  $\tilde{G}$ . In Fig. 14 we show the Higgsino and photino components of the  $\tilde{\chi}_1^0$ . In Figs. 14(a) and 14(b) we set  $n_5 = 1$  and see that the NLSP is approximately 60 to 90% (40% to 70%) photino for  $\mu > 0$  ( $\mu < 0$ ). The Higgsino component is quite small. The Higgsino component can be larger if  $n_5$  is larger, because  $|\mu|$  is reduced relative to the gaugino masses. In Fig. 14(c) we see that for  $n_5 = 4$  and  $\mu > 0$ , the Higgsino component of the NLSP can be large. In fact, it can be as large as 50%.

The  $\tilde{\chi}_i^0$  partial widths can be readily computed. We express them in units of

$$\mathcal{A} = \frac{m_{\tilde{\chi}_i^0}^5}{96\pi M_G^2 M_P^2} = \frac{m_{\tilde{\chi}_i^0}^5}{16\pi F_S^2}. \quad (11)$$

We first write the well-known decay rate to a photon and the gravitino,

$$\mathcal{A}^{-1} \Gamma(\tilde{\chi}_i^0 \rightarrow \tilde{G} \gamma) = 2 \kappa_{i\gamma}. \quad (12)$$

For the remaining decay modes, we give the three body decay formula to account for the

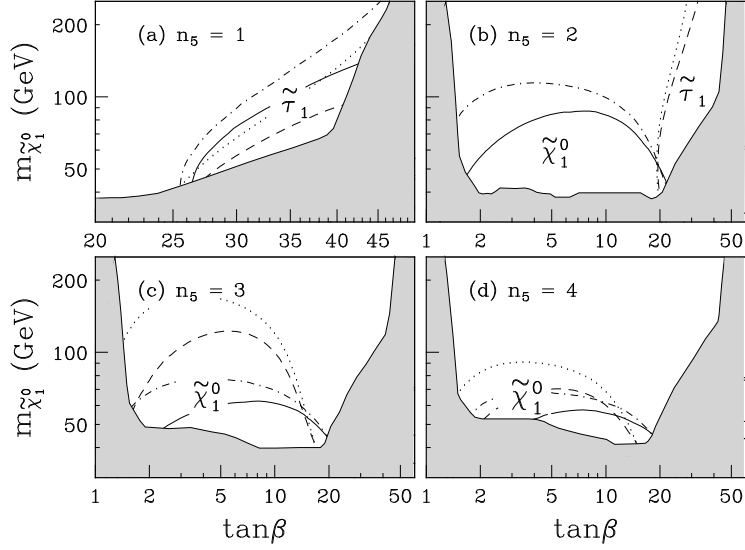


Figure 12: Contours marking the boundary where the mass of the light tau slepton is equal to the mass of the lightest neutralino, for  $n_5 = 1, 2, 3$  and  $4$ . The solid (dashed) line corresponds to  $\mu > 0$ ,  $M/\Lambda = 2$  ( $10^4$ ). The dot-dashed (dotted) line corresponds to  $\mu < 0$ ,  $M/\Lambda = 2$  ( $10^4$ ). The excluded region is plotted for  $\mu > 0$  and  $M/\Lambda = 2$ . The label  $\tilde{\chi}_1^0$  ( $\tilde{\tau}_1$ ) marks the region where the neutralino (tau slepton) is the NLSP.

decay to standard model fermions via real or virtual boson exchange. If we sum over final-state standard-model fermions, we find

$$\begin{aligned}
\mathcal{A}^{-1} \Gamma(\tilde{\chi}_i^0 \rightarrow \tilde{G} f^+ f^-) &= 2\kappa_{iZ_T} I_1(Z) + \kappa_{iZ_L} I_0(Z) \\
&+ 80s_W c_W \left[ \frac{3 - 8s_W^2}{63 - 120s_W^2 + 160s_W^4} \right] \kappa_{iZ_\gamma} (I_1(Z) - I_0(Z)) \\
&+ \kappa_{i\gamma} \frac{40\alpha}{9\pi} \left( -\frac{25}{12} - \ln \frac{s_{\min}}{m_{\tilde{\chi}_i^0}^2} \right) \\
&+ \sum_{\varphi=h,H,A} \text{BR}(\varphi \rightarrow f^+ f^-) \kappa_{i\varphi} I_1(\varphi) \\
&- 2 \left[ \text{BR}(h \rightarrow f^+ f^-) \text{BR}(H \rightarrow f^+ f^-) \right]^{\frac{1}{2}} \kappa_{iHh} I_{10}(h, H),
\end{aligned} \tag{13}$$

where  $s_{\min}$  is the minimum experimentally detectable fermion invariant mass, and

$$\begin{aligned}
\kappa_{i\gamma} &= |N_{i1}c_W + N_{i2}s_W|^2, \\
\kappa_{iZ_T} &= |N_{i2}c_W - N_{i1}s_W|^2, \\
\kappa_{iZ_\gamma} &= c_W s_W (|N_{i2}|^2 - |N_{i1}|^2) + (c_W^2 - s_W^2) \text{Re}(N_{i1}^* N_{i2}), \\
\kappa_{iZ_L} &= |N_{i3}c_\beta - N_{i4}s_\beta|^2, \\
\kappa_{iA} &= |N_{i4}c_\beta + N_{i3}s_\beta|^2, \\
\kappa_{iH} &= |N_{i3}c_\alpha + N_{i4}s_\alpha|^2, \\
\kappa_{ih} &= |N_{i4}c_\alpha - N_{i3}s_\alpha|^2,
\end{aligned} \tag{14}$$



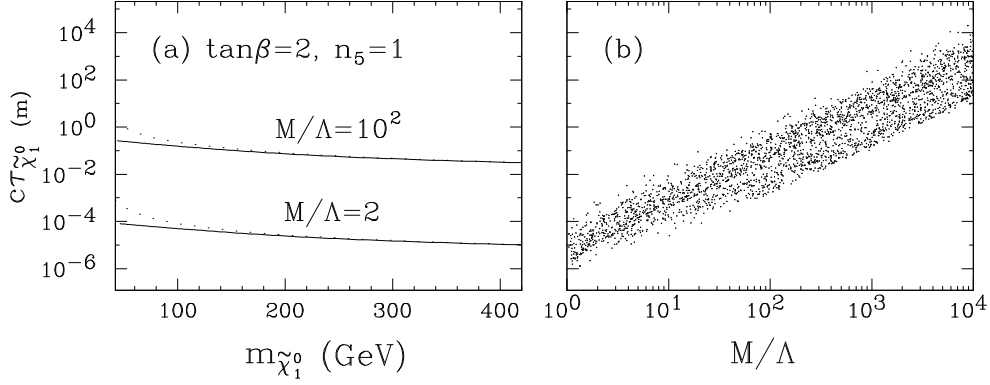


Figure 13: (a) The lifetime of the NLSP, for  $\tan\beta = 2$  and  $n_5 = 1$ , with  $\mu > 0$  (solid line) or  $\mu < 0$  (dotted). For fixed  $m_{\tilde{\chi}_1^0}$ , the lifetime scales like  $(M/\Lambda)^2$ . (b) A scatter plot of the neutralino lifetime, restricted to cases where the neutralino is the NLSP.

$$\kappa_{iHh} = s_\alpha c_\alpha \left( |N_{i4}|^2 - |N_{i3}|^2 \right) + (c_\alpha^2 - s_\alpha^2) \mathcal{R}e(N_{i3}^* N_{i4}) .$$

In writing the  $H$ - $h$  interference contribution, we have neglected all Yukawa couplings except those of the the bottom and tau.

In these expressions, the integrals  $I_n$  are given by

$$I_n(\varphi) = \frac{\epsilon_\varphi}{\pi} \int_0^1 dx \frac{(1-x)^4 (x/R_\varphi)^n}{(x-R_\varphi)^2 + \epsilon_\varphi^2} , \quad (15)$$

with  $R_\varphi = M_\varphi^2/m_{\tilde{\chi}_i^0}^2$  and  $\epsilon_\varphi = \Gamma_\varphi M_\varphi/m_{\tilde{\chi}_i^0}^2$ . These integrals reduce to  $(1-R_\varphi)^4$  for small  $\epsilon_\varphi$  (i.e. in the narrow width approximation). The integral  $I_{10}(h, H)$  is

$$I_{10}(h, H) = \frac{1}{\pi} \sqrt{\frac{\epsilon_h \epsilon_H}{R_h R_H}} \int_0^1 dx \frac{x(1-x)^4 \left[ (x-R_H)(x-R_h) + \epsilon_h \epsilon_H \right]}{((x-R_h)^2 + \epsilon_h^2) ((x-R_H)^2 + \epsilon_H^2)} . \quad (16)$$

Our results complete the formulae for the two-body decay rates of the  $\tilde{\chi}_i^0$  given in ref. [3]. Our results include the contribution of the virtual photon and the contributions from  $Z$ - $\gamma$  and  $H$ - $h$  interference. Note that our formula for  $\Gamma(\tilde{\chi}_i^0 \rightarrow \tilde{G} + \text{Higgs boson})$  does not agree with that of ref. [3]. In particular, our result contains the function  $I_1$ , not  $I_0$ . At first sight one might conclude that this violates the electroweak equivalence theorem, since the decay rate to the longitudinal  $Z$  ( $\sim I_0$ ) is not equal to the decay rate to the Goldstone boson ( $\sim I_1$ ). However, the equivalence principle does indeed hold in the applicable regime, since the two functions approach each other for  $m_{\tilde{\chi}_i^0} \gg M_Z$ .

In Fig. 15(a) we show the branching fractions of the  $\tilde{\chi}_1^0$  versus  $m_{\tilde{\chi}_1^0}$ , for  $\tan\beta = 2$ ,  $n_5 = 1$ , and  $M = 2\Lambda$ . (We plot the magnitude of the  $Z$ - $\gamma$  interference contribution,  $|\Gamma_{Z\gamma}|/\Gamma_{\text{tot}}$ .) The decay to the photon dominates, as expected, since the  $\tilde{\chi}_1^0$  has a large photino component. The branching fraction to fermions via an off-shell photon varies from about 3 to 4% with  $s_{\min} = 1$  GeV.

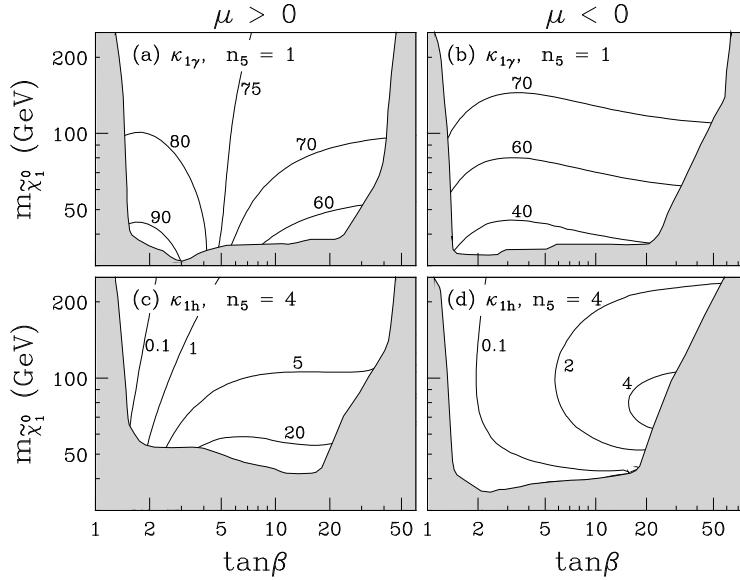


Figure 14: Figures (a) and (b) [(c) and (d)] show the photino component of the lightest neutralino,  $\kappa_{1\gamma}$  [the Higgsino component,  $\kappa_{1h}$ ], in per cent, for  $M/\Lambda = 2$  and  $n_5 = 1$  [ $n_5 = 4$ ].

In the parameter space associated with the minimal models, the branching ratio to fermion pairs via heavy Higgs boson exchange is negligible. For the parameters corresponding to Fig. 15, the heavy Higgs exchange branching ratio is of order  $10^{-12}$ . The branching ratio associated with  $H$ - $h$  interference and the branching fraction associated with virtual  $h$ -boson exchange are about an order of magnitude larger.

Because of the  $\beta^8$  suppression, the branching fraction to the  $Z$ -boson rises slowly above threshold, to about 15% (20%) for  $m_{\tilde{\chi}_1^0} = 2M_Z$  ( $3M_Z$ ). We illustrate this in Fig. 15(b), where we show a scatter plot of the branching fraction of the lightest neutralino to a gravitino and a fermion pair. We see that the branching ratio depends only on the neutralino mass. This would not be true if the part of parameter space in which the  $\tilde{\chi}_1^0$  has a large Higgsino component ( $n_5 = 4$ ,  $\mu > 0$ , small  $\Lambda$ , see Fig. 14(c)) led to a sizable branching ratio to the Higgs boson. However, in this region of parameter space either the  $\tilde{\tau}_1$  is the NLSP or the  $\tilde{\chi}_1^0$  mass is below the  $h$ -boson threshold. Hence, the associated partial width is negligible.

As discussed above, the mechanism that generates  $B(M)$  and  $\mu(M)$  might result in extra terms to the scalar masses beyond those in eq. (4). In this case, the NLSP can decay predominately into a Higgs boson. To study this possibility, we take  $\mu$  and  $B$  to be independent low-energy parameters, and focus our attention on the case of small  $\mu$ , so the lightest neutralino is predominantly Higgsino. In Fig. 16 we plot the lifetime and branching fractions of the  $\tilde{\chi}_1^0$  as a function of  $m_{\tilde{\chi}_1^0}$ , for various choices of parameters. Note that in the region  $m_{\tilde{\chi}_1^0} \lesssim 250$  GeV the lightest neutralino is largely Higgsino, and  $m_{\tilde{\chi}_1^0} \simeq |\mu|$ .

The lifetime and branching fractions of the NLSP in the Higgsino region are shown in Fig. 16. In Fig. 16(a) we see that the lifetime varies by 6 or 7 orders of magnitude as  $m_{\tilde{\chi}_1^0}$  varies over less than one order of magnitude. This can be contrasted with the case where the neutralino is dominantly  $B$ -ino, where the lifetime varies by less than one order of magnitude (see eq. (9) and Fig. 13). The branching fractions of the lightest neutralino are shown in

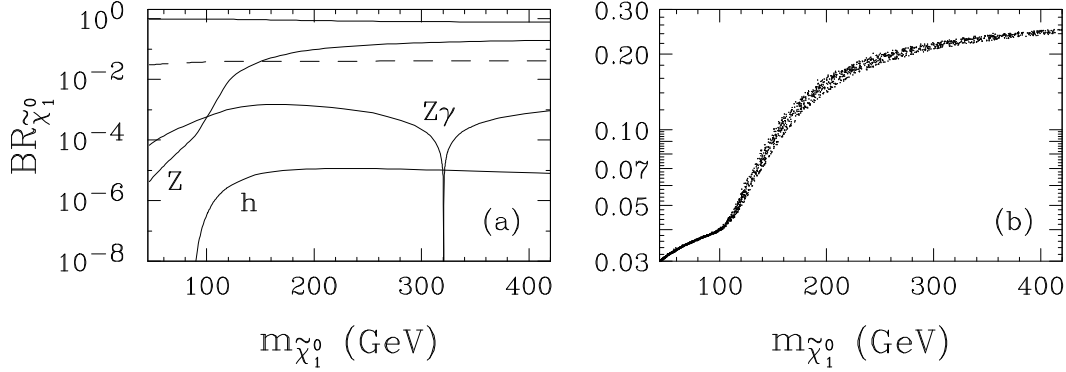


Figure 15: (a) The branching ratios of the  $\tilde{\chi}_1^0$  in the case  $M/\Lambda = 2$ ,  $n_5 = 1$  and  $\mu > 0$ . The solid line near 1 is the branching ratio to a photon and the gravitino, and the dashed line is the branching ratio to leptons via a virtual photon. (b) A scatter plot of the neutralino branching fraction to fermion pairs, in the cases where the neutralino is the NLSP.

Figs. 16(b-d).

These results can be understood as follows. In the small  $\mu$  region the NLSP is primarily Higgsino, so it prefers to decay to a Higgs boson. Below  $h$  and  $Z$  threshold, however, it is forced to decay through its suppressed photino component. This accounts for the long lifetime and the large photino branching fraction for small  $m_{\tilde{\chi}_1^0}$ . As the mass increases, the  $h$  and  $Z$  channels open, so the lifetime increases and the branching fractions are determined by  $\kappa_{1Z_L}$  and  $\kappa_{1h}$ . For small  $\tan\beta$ , the decay to  $h$  ( $Z$ ) dominates for  $\mu$  positive (negative). For large  $\tan\beta$ ,  $\kappa_{1Z_L} \simeq \kappa_{1h}$  for each sign of  $\mu$ . In this case the branching fraction to  $Z$  is larger because the Higgs is heavier, so  $I_0(Z) > I_1(h)$ . Finally, as  $m_{\tilde{\chi}_1^0}$  increases still further, the decay to photons again dominates, because in this region, the NLSP is predominately photino. For  $m_{\tilde{\chi}_1^0} \simeq 300$  GeV, the decay length approaches  $10^{-5}$  meters.

The neutralino lifetime in the Higgsino region can be readily scaled for other values of  $n_5$  and  $M/\Lambda$ . As before, for fixed  $m_{\tilde{\chi}_1^0}$ ,  $c\tau$  scales like  $(M/\Lambda)^2$ . For fixed  $M/\Lambda$  and fixed gaugino masses, it scales like  $1/n_5^4$  (see eq. (9)).

These results should be contrasted with those of the minimal models, where we found that, above  $h$  threshold, the branching ratio to the  $h$  varies from  $10^{-8}$  to  $10^{-4}$ . Therefore collider events with four  $b$ -jets and missing energy would imply a non-minimal Higgs sector in these models.

## 5 Conclusions

In this paper we examined the detailed low-energy spectrum of gauge-mediated supersymmetry breaking models. We used two-loop renormalization group equations for the gauge and Yukawa couplings, and for the soft supersymmetry breaking parameters. We imposed consistent one-loop radiative electroweak symmetry breaking under the assumption that the mechanism that generates the  $\mu$  and  $B$  parameters does not induce any extra contributions

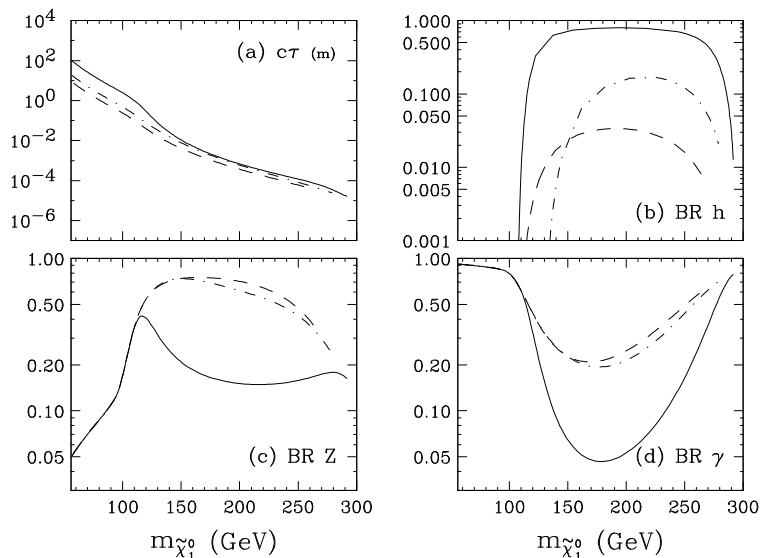


Figure 16: The (a) lifetime and (b-d) branching fractions of the NLSP, for the case where the  $\tilde{\chi}_1^0$  is primarily Higgsino. All plots are for  $n_5 = 1$  and  $\Lambda = 200$  TeV. The  $m_{\tilde{\chi}_1^0}$  values are obtained by varying  $\mu$  from 50 to 350 GeV. The solid (dashed) lines are for  $\tan \beta = 2$ , with  $\mu$  positive (negative). The dot-dashed lines correspond to  $\tan \beta = 40$ ,  $\mu > 0$ . (The curves for  $\tan \beta = 40$ ,  $\mu < 0$  are almost identical.)

to the scalar masses.

We examined the phenomenology in the case of an arbitrary number of  $5 + \bar{5}$  messenger fields, and in the case that the messenger scale  $M$  is greater than  $\Lambda$ . We began by examining electroweak symmetry breaking. We initially considered the minimal case,  $n_5 = 1$  and  $M = 2\Lambda$ . In the parameter space we considered, with  $\Lambda < 300$  TeV, we found that  $|\mu(M)|$  varies from 150 GeV to over 1 TeV. We also found that  $|B(M)/\mu(M)|$  varies from near (but not equal to) zero to about 500 GeV. We found the phenomenologically interesting region  $B(M) \simeq 0$  to be compatible with electroweak symmetry breaking in the region of large  $\tan \beta$ , for either sign of  $\mu$ . For larger  $M/\Lambda$ , we found  $B(M) \simeq 0$  requires  $\mu < 0$ .

We examined the spectrum and illustrated how it depends on  $n_5$  and  $M/\Lambda$ . We found that the spectrum is not qualitatively affected by an increase in  $M/\Lambda$ . For  $n_5 > 1$ , we found that the light tau slepton is the NLSP over most of the parameter space. It decays to a tau lepton and a gravitino.

By varying the boundary conditions of the soft parameters at the messenger scale by 5%, we determined the sensitivity of the supersymmetric spectrum to higher-order messenger-sector corrections. We found that in the region  $B(M) \simeq 0$ ,  $B(M)$  varies by 10 GeV. Furthermore, the spectrum varies by 5%, except for the light Higgs mass, which is essentially unchanged, and the third-generation squark and slepton masses. In the most extreme case, we found a 70% variation in the light tau slepton mass, which implies a substantial uncertainty in the identification of the NLSP.

We compared the predictions for the spectra in the gauge-mediated and supergravity-inspired models. In general, the two models predict qualitatively different spectra. We found that it is possible for the two models to give the same gluino, light chargino, and (first and

second generation) squark and slepton masses. Such a match is only possible for very light masses, where  $D$ -terms and gaugino/Higgsino mixing is important. In this region, the models can be distinguished by their predictions for other observables, such as  $\tan\beta$ , as well as the sneutrino, neutralino, heavy chargino, and Higgs boson masses.

For  $n_5 = 1$ , we found that the  $\tilde{\chi}_1^0$  is usually the NLSP. The  $\tilde{\chi}_1^0$  decays to the gravitino and either an (on- or off-shell) gauge or Higgs boson. We derived the neutralino decay rate and branching fractions. The lightest neutralino tends to be gaugino-like, and decays to a photon and a gravitino. However, in the region  $m_{\tilde{\chi}_1^0} \gtrsim 100$  GeV, the branching fraction to the  $Z$  can be larger than 20%. Leptons are easier to track than photons, so this mode has the potential to permit a precise neutralino lifetime measurement. We found that for  $n_5 = 4$  the Higgsino component of the  $\tilde{\chi}_1^0$  can be as large as 50%. Nevertheless, over the entire parameter space the branching fraction to the light Higgs boson is less than  $10^{-4}$ .

We also examined the branching fraction of the neutralino in the Higgsino region. In this case the branching fraction to the on-shell  $h$ -boson can reach over 80% well above threshold. Since this Higgsino region can only occur for models with non-minimal Higgs sectors, the observation of 4  $b$ -jets plus missing energy would be an important step towards understanding the origin of the  $\mu$  term.

Models with gauge-mediated supersymmetry breaking offer the appealing possibility that the origin of supersymmetry breaking is experimentally accessible. Once supersymmetry is discovered, detailed study of the supersymmetric particles, along the lines suggested here, might well prove to be the first step towards uncovering the mechanism of supersymmetry breaking.

## Acknowledgements

One of us (D.M.P.) thanks Scott Thomas and James Wells for useful conversations and comparisons.

## References

- [1] M. Dine and A. Nelson, *Phy. Rev. D* **47**, 1277 (1993); M. Dine, A. Nelson and Y. Shirman, *Phys. Rev. D* **51**, 1362 (1995); M. Dine, A. Nelson, Y. Nir and Y. Shirman, *Phys. Rev. D* **53**, 2658 (1996).
- [2] D.R. Stump, M. Wiest and C.P. Yuan, *Phys. Rev. D* **54**, 1936 (1996); S. Dimopoulos, M. Dine, S. Raby and S. Thomas, *Phys. Rev. Lett.* **76**, 3494 (1996); S. Ambrosanio, G.L. Kane, G.D. Kribs, S.P. Martin and S. Mrenna, *ibid* **76**, 3498 (1996); *ibid* hep-ph/9607414; S. Dimopoulos, S. Thomas and J.D. Wells, hep-ph/9604452.
- [3] S. Ambrosanio, G.L. Kane, G.D. Kribs, S.P. Martin and S. Mrenna, hep-ph/9605398.
- [4] S.P. Martin, hep-ph/9608224.
- [5] C. Carone and H. Murayama, *Phys. Rev. D* **53**, 1658 (1996).
- [6] S. Dimopoulos, G.F. Giudice and A. Pomarol, preprint CERN-TH/96-171, hep-ph/9607225.

- [7] T. Gherghetta, G. Jungman and E. Poppitz, preprint UM-TH-95-27, hep-ph/9511317; G. Dvali, G.F. Giudice and A. Pomarol, preprint CERN-TH/96-61, hep-ph/9603238.
- [8] M. Dine, Y. Nir and Y. Shirman, preprint SCIPP-96-30, hep-ph/9607397.
- [9] K. Babu, C. Kolda and F. Wilczek, preprint IASSNS-HEP 96/55, hep-ph/9605408.
- [10] T. Hotta, K.-I. Izawa and T. Yanagida, preprint UT-752, hep-ph/9606203.
- [11] I. Dasgupta, B.A. Dobrescu and L. Randall, preprint BUHEP-96-25, hep-ph/9607487.
- [12] M. Dugan, B. Grinstein and L. Hall, Nucl. Phys. B **255**, 413 (1985); S. Dimopoulos and S. Thomas, Nucl. Phys. B **465**, 23 (1996).
- [13] D. Pierce, J. Bagger, K. Matchev and R.-J. Zhang, preprint SLAC-PUB-7180, JHU-TIPAC-96011, hep-ph/9606211.
- [14] H. Pagels and J.R. Primack, Phys. Rev. Lett. **48**, 223 (1982).